Applied Catalysis A: General 407 (2011) 134–144

Contents lists available at SciVerse ScienceDirect

Applied Catalysis A: General

journal homepage: www.elsevier.com/locate/apcata

AgNaMordenite catalysts for hydrocarbon adsorption and deNO$_x$ processes

Soledad G. Aspromonte, Ramiro M. Serra, Eduardo E. Miró, Alicia V. Boix*

Instituto de Investigaciones en Catálisis y Petroquímica – INCAPE (FIQ, UNL-CONICET), Santiago del Estero 2829, 3000, Santa Fe, Argentina

ARTICLE INFO

Article history:
Received 19 May 2011
Received in revised form 17 August 2011
Accepted 21 August 2011
Available online 26 August 2011

Keywords:
Toluene adsorption
Butane adsorption
SCR-NO$_x$
AgNaMordenite

ABSTRACT

Silver catalysts were prepared by ion exchange of NaMordenite with 5, 10 and 15 wt% Ag. Various characterization techniques such as TPR, UV–vis and XPS indicated the presence of small particles of highly dispersed Ag_2O together with isolated Ag^+ cations located in α, β and γ exchange sites of NaMOR. The formation of clusters of cationic silver (Ag_n^{m+}) was also considered.

The prepared samples were active in the Selective Catalytic Reduction of NO$_x$ in the presence of toluene or butane as reducing agents, excess oxygen and 2% H_2O. The solid with 15 wt% Ag was the most active one in the presence of water, reaching a maximum conversion of NO$_x$ to N_2 of 47.5% or 51.2% when butane or toluene were respectively used. Under dry conditions, the maximum conversion of NO had an optimum between 5 and 10 wt% Ag for both hydrocarbons.

The NaMOR support showed a higher adsorption capacity than the exchanged samples with both hydrocarbons. For the silver loaded solids, the toluene adsorption capacity at 100 °C increased with the increase of the metal content. In contrast, the amount of butane adsorbed was similar for the different contents of Ag. Consequently, silver has two opposite effects: one is the partial obstruction of the mordenite channels, as seen by the loss of crystallinity and the decrease of surface area and pore volume; and the other effect is the chemical interaction that depends on the nature of the adsorbed hydrocarbon. The interaction between toluene and Ag^+ ions is stronger with the π-electrons of the aromatic ring of the toluene molecule than with the σ-electrons of the linear chain of butane. For this reason, toluene is retained at higher temperatures than butane. In addition, between 300 and 500 °C, the appearance of signals corresponding to H_2, CO_2 and H_2O is observed during the TPD of toluene. This indicates that the toluene decomposition occurs, producing coke and hydrogen. Most probably, the generation of CO_2 and H_2O is a consequence of the reduction of Ag_2O particles with toluene.

1. Introduction

Air pollution is mainly due to the emission of nitrogen oxides (NO, NO_2), carbon oxides (CO, CO_2), unburnt hydrocarbons (HCs), particulate matter (PM) and volatile organic compounds (VOCs) from power plants, chemical and petrochemical plants, and vehicles. The Selective Catalytic Reduction (SCR) using HCs as reducing agent is one interesting way which allows NO$_x$ abatement under oxidizing conditions [1–3]. An important issue for automobile catalyst manufacturers is the study of contaminant abatement under conditions close to real behavior. In this sense, it is important to take into account a possible effect of the presence of other compounds such as H_2O and unburnt hydrocarbons. In fact, during the engine cold-start, 80% of the unburned hydrocarbons are emitted to the atmosphere through the converter without reacting. In addition, the three-way catalysts (TWC) are weak or inactive at low temperatures and require temperatures above 300 °C to have an optimal performance. For these reasons, it is necessary to implement new systems aimed at reducing these emissions [4–6].

An interesting alternative consists in the combination of the excellent adsorption properties of zeolite materials with the high catalytic activity of exchange cations such as Co, Fe, In, Ag and Cs, in the Selective Catalytic Reduction of NO$_x$ using adsorbed HC as a reducing agent [7–9]. Thus, this is a promising system able to adsorb HCs at low temperature and to reduce NO$_x$ at the normal operating temperature of the converter. Given this situation, it is clear that the study of a combined adsorption of hydrocarbon with nitrogen oxides reduction is a major issue.

In this vein, some HCs adsorption and desorption experiments have been reported on various zeolites such as BEA [10], Ferrierite [11] and H-ZSM5 [12]. The adsorption capacity of zeolite materials depends on several factors, namely, the quantity, accessibility and distribution of active sites, as well as the topology of the zeolite. Specifically, in the Na-mordenite zeolites the substitution of a Si^{4+} ion by an Al^{3+} ion with a lower valence produces a negative charge on the structure that is neutralized by the Na^+ cation forming a conjugate acid–base pair. The Na^+ cation acts as a Lewis acid site, while the oxygen of the zeolite structure with partial negative charge acts

* Corresponding author. Tel.: +54 03424536861.
E-mail address: aboix@fiq.unl.edu.ar (A.V. Boix).

0926-860X/$ – see front matter © 2011 Elsevier B.V. All rights reserved.
doi:10.1016/j.apcata.2011.08.033

as a Lewis base. Thus, the cations in Na-mordenite are adsorption sites for molecules with π electrons and many compounds of this type have been studied, particularly benzene. The two main modes of benzene adsorption involve two interactions, one between its π electron cloud with the counter-ions and another between the CH group with framework oxygen bearing the negative charge of the lattice [13].

This is supplemented by several investigations which have studied the catalytic properties of silver catalysts for the SCR-NO_x with different hydrocarbons [14,15]. Silver-alumina (Ag/Al_2O_3) catalysts have been widely explored due to their ability to reduce NO_x with HCs and H_2 [16–18]. Farrauto et al. [19] found that Ag-ZSM-5 was a good candidate of HC trapping materials under cold-start conditions and other authors tested thiophene on NaY zeolite exchanged with Ni^{2+}, Ag^+ and Zn^{2+} [20]. In the same way, Kaliaguine et al. [21] reported that the Ag-ZSM-12 catalyst was a promising adsorbent due to its low sensitivity to H_2O and CO_2 which are essentially present in the exhaust stream of vehicles. Elangovan et al. [22] used MCM-68 and SSZ-33 exchanged with Ag^+, Co^{2+} and Mg^{2+} as hydrocarbon trap. Therefore, the presence of Ag seems to be important for the combination of adsorption/desorption and SCR-NO_x processes.

The purpose of this work was to study the behavior of Ag-NaMordenite catalysts in the Selective Catalytic Reduction of NO_x with hydrocarbons. Basic studies were performed on the adsorptive and catalytic properties of these materials. Two different HC specifications were considered: butane as a saturated short HC and toluene, representative of the aromatic family.

The catalysts were prepared with different loadings of silver and they were thoroughly characterized by temperature-programmed reduction (TPR), X-ray diffraction (XRD), UV–vis diffusive-reflectance (UV–vis DRS) and X-ray photoelectron spectroscopy (XPS).

2. Experimental

2.1. Catalyst preparation

The ion-exchange method generally results in a strong metal-support interaction and a better dispersion of metal in the zeolite. Hence, this method was applied to incorporate silver into a commercial sodium-type mordenite zeolite sample (NaMOR, $SiO_2/Al_2O_3 = 13$) provided by Zeolyst International. In this procedure, 4 g of the zeolite powder were added to 150 ml of $AgNO_3$ solution with concentrations from 0.04 to 0.10 M. The mixture was then stirred at 25 °C for 24 h. All the above procedures were performed in the dark due to the sensitivity of silver to the light. The suspension was then filtered and dried at 80 °C, followed by treatment in O_2 flow at 500 °C. The calcined samples were denoted as Ag(*x*)M, where '*x*' was the percent by weight of silver. The silver loadings were 5, 10 and 15 wt% determined by atomic absorption spectrometry flame (AASF), which corresponded to ion-exchange degrees of 17.8, 35.5 and 53.1%, respectively. It was assumed that each monovalent Na^+ ion was exchanged with one monovalent Ag^+ ion.

A mechanical mixture was prepared between Ag_2O and NaMOR, known as Ag_2O/M and used as reference sample in some of the characterization techniques (XPS, TPR and UV–vis).

2.2. Catalyst characterization

2.2.1. Determination of pore volume and surface area

Nitrogen adsorption–desorption isotherms were obtained at −196 °C on a Quantachrome Autosorb instrument. Previously, the samples were outgassed at 300 °C for 6 h (10^{-4} Torr). The Brunauer–Emmett–Teller (BET) equation was used for calculating the specific surface area of the materials from N_2 adsorption isotherms. The micropore volume was determined by applying the *t*-plot method [23].

2.2.2. X-Ray diffraction

This technique was employed for the detection of metallic Ag, Ag_2O and to determine the crystallinity of the Ag(*x*)M catalysts. The X-ray diffraction measurements were taken using an XD-D1 model Shimadzu diffractometer operated with Cu Kα radiation at 30 kV and 40 mA, using a scanning rate of $1^\circ\,min^{-1}$. The database employed was the one provided by the manufacturer. The crystallinity was estimated from the ratio of the sum of the intensity of the prominent peaks corresponding to planes (1 1 1), (3 3 0), (1 5 0), (2 0 2) and (3 5 0) of Ag(*x*)M samples and NaMOR support. The maximum degree of crystallinity was taken equal to 100% and corresponded to calcined NaMOR [24].

2.2.3. Temperature-programmed reduction

The TPR experiments were performed using an Okhura TP-2002-S instrument equipped with a TCD detector. A mixture of 30 ml min^{-1} of 5% H_2 in Ar was used. The heating rate was 10 °C min^{-1} up to 900 °C. Fresh samples were pre-treated in O_2 flow in situ, heating at 5 °C min^{-1} from room temperature up to 500 °C and kept at that temperature for 2 h. The amount of Ag(*x*)M samples was 0.10 g. The H_2 consumption was referred to the silver content of the prepared samples.

2.2.4. Diffusive-reflectance UV–vis experiments

UV–vis spectra were collected on a Shimadzu UV–vis–NIR model UV-3600 spectrophotometer, with the use of a diffusive-reflectance attachment with an integrating sphere coated with $BaSO_4$. Diffuse reflectance spectra (DRS) were registered for samples storage under ambient conditions. $BaSO_4$ was used as a reference. The absorption intensity was calculated from the Schuster–Kubelka–Munk equation, $F(R_\infty) = (1 - R_\infty)^2/2R_\infty$, where R_∞ is the reflectance.

2.2.5. X-Ray photoelectron spectroscopy

The XPS measurements were performed with the multitechnique system (SPECS) equipped with a dual X-ray source and a hemispherical PHOIBOS 150 analyzer operating in the fixed analyzer transmission (FAT) mode. The spectra were obtained with pass energy of 30 eV and Mg Kα radiation ($h\nu = 1253.6$ eV) operated at 200 W and 12 kV. The working pressure in the analyzing chamber was less than 5.9×10^{-7} Pa. The binding energies (BE) of core-levels Si 2p, Al 2p, Ag 3d, C 1s, O 1s, and the kinetic energy (KE) in the region of the Ag M_4VV Auger transitions were measured. The Si 2p peak at 102.4 ± 0.1 eV of binding energy (BE) was taken as internal reference.

The binding energy positions of Ag 3d do not identify the oxidation state of the silver species, because the characteristic states of oxidized (Ag_2O) and metallic silver (Ag°) are close together (within 0.5 eV) [25]. Thus, the modified Auger parameter (α') was used to characterize the chemical state of Ag. This parameter is the sum of the kinetic energy of the Auger electron (AgM_4VV) and the binding energy of the core-level ($Ag\,3d_{5/2}$) peak. This parameter is independent of charging, but still sensitive to chemical shifts.

The data treatment was performed with the Casa XPS program (Casa Software Ltd., UK). The peak areas were determined by integration employing a Shirley-type background. Peaks were considered to be a mixture of Gaussian and Lorentzian functions in a 70/30 ratio. For the quantification of the elements, sensitivity factors provided by the manufacturer were employed.

2.3. Catalytic tests

The performance of catalysts in the Selective Catalytic Reduction of NO with toluene or butane was evaluated in a continuous flow system. The reaction mixture typically contained 1000 ppm NO, 500 ppm butane or toluene, 2% O_2 and 2% H_2O (balanced He) with a gas hourly space velocity, GHSv = 20,000 h^{-1}. Conversion profiles were obtained by increasing the temperature in steps of 50 °C and monitoring concentrations for 60–90 min at each temperature. The concentration of gases was analyzed with a Shimadzu GC-2014 chromatograph equipped with a thermal conductivity detector (TCD) and a Zeolite 5A molecular sieve column at 45 °C.

2.4. Hydrocarbons adsorption and temperature-programmed desorption experiments

Experiments were performed to determine the HCs adsorption and retention capacities. Toluene and butane were used as representative aromatic and linear molecules, respectively.

Adsorption and desorption experiments were carried out in a continuous flow system. The stream of toluene diluted in He was obtained by passing pure He through two connected saturators that contained liquid C_7H_8 (99.9%, Sigma–Aldrich). The temperature of saturators was kept at 0 °C with an ice bath which allowed obtaining approximately 8000 ppm of toluene. The sample (ca. 100 mg) was placed in a tubular quartz reactor of ca. 5 mm i.d., which was placed inside an electrical furnace equipped with a temperature controller. Subsequently, the sample was dehydrated in an inert flow at 500 °C for about 6 h. After cooling the solid sample to 100 °C, it was exposed to C_7H_8/He flow during 1 h before the TPD experiments. The butane adsorption was carried out with 10,000 ppm of butane in He flow and the breakthrough curves at 100 °C were obtained for calcined Ag(*x*)M catalysts.

Both toluene and butane experiments were carried out in He flow (25 ml min^{-1}). Before the TPD experiments, a sweep under He flow at 100 °C was carried out. The temperature-programmed desorption was performed from 100 to 550 °C with a rate of 5 °C min^{-1} and maintaining it at the final temperature for about 10 min. The effluent gases were continuously monitored by on-line mass spectrometry (Pfeiffer/Balzers Quadstar, QMI422, QME125). The toluene concentration (m/e = 91) and the signal m/e = 43 which corresponds to the main partition of butane was registered through mass spectrometry. In addition, several other signals such as 2 (hydrogen), 4 (helium), 28 (nitrogen or CO), 32 (oxygen), 105 (benzoic acid), 44 (CO_2), 77 (phenyl), 18 (water), 62 (pentene), 15 (methyl group) and 16 (methane) were monitored [26].

The amount of toluene or butane adsorbed during the breakthrough experiments (adsorption capacity) was calculated as the difference between the area under the curve in a blank experiment and the area under the breakthrough curve. We also measured the area under the curve during the TPD experiments, from which we were able to calculate the amount of toluene or butane desorbed between 100 and 550 °C. This amount corresponds to the toluene or butane retained in the sample after purging with He at 100 °C.

3. Results and discussion

3.1. Catalyst characterization

3.1.1. Physical and chemical properties of Ag(x)M catalysts

Table 1 shows the chemical composition of NaMOR and Ag(*x*)M determined by atomic absorption spectroscopy; it also shows the BET area and micropore volume. The surface area value of NaMOR is in agreement with that reported by the zeolite supplier [27]. The incorporation of silver by ion-exchange into the mordenite channels decreases the surface area and pore volume compared with the parent zeolite. In addition to the incorporation of Ag, the ion exchange process also results in the exchange of a fraction of Na by protons, which can be inferred from the Na concentration of each sample, which is also shown in Table 1.

Table 1
Textural properties of NaMOR exchanged with silver.

Catalyst	Ag (wt%)	Na (wt%)	S_{BET}[a]	V_μ[b]	Crystallinity[c] (%)
NaMOR	0	4.1	409	0.165	100.0
Ag(5)M	5	1.2	265	0.083	77.9
Ag(10)M	10	0.5	301	0.088	58.9
Ag(15)M	15	0.3	309	0.086	36.6

[a] Calculated from N_2 isotherms at (−196 °C) (m^2 g^{-1}).
[b] Micropore volume (cm^3 g^{-1}) calculated by *t*-plot method.
[c] Crystallinity calculated using the ratio of the sum of the intensity of the five most intense of Ag(*x*)M and NaMOR.

In the Ag(*x*)M samples only the diffraction peaks belonging to the NaMOR structure were detected by XRD measurements. Since the diffraction lines of Ag_2O (2θ = 32.6°, 37.8°, 54.7° and 65.3°) are clearly seen on the Ag_2O/M reference sample [28], in the exchanged sample the Ag_2O particles should be highly dispersed in the mordenite structure.

The crystallinity of the Ag(*x*)M samples decreased with the increase of the silver ion-exchanged degree (Table 1). The X-ray diffraction patterns (not shown) of Ag(*x*)M presented some changes in the relative intensities, probably due to the incorporation of silver in the structure by the ion-exchange procedure. Kukulska-Zaja and Datka [29] reported that the location of silver in the oxygen ring results in ring deformation which increases with the number of cations incorporated in the cavities. Thus, the increased number of Ag^+ ions in the zeolitic cavities would cause some distortions in the pore and intracrystalline voids due to interaction with the lattice oxygen.

3.1.2. Reducibility of Ag species

The properties of the active sites are related to the different species of Ag present in the catalysts. Temperature-programmed reduction helps in differentiating these species. Fig. 1 shows the results obtained by TPR for Ag(*x*)M catalysts and for the standard sample. The reduction profiles exhibit peaks in three temperature regions which can be attributed to different silver species formed during the pretreatment step. One hypothesis is to consider that these peaks correspond to the reduction of isolated silver ions multi-coordinated with structure oxygens. It is known that the occupation of different sites in mordenite by metallic cations depends on several factors. Whichterlová and co-workers [30,31] identified three cationic sites in Co-exchanged mordenite. They found that when the cobalt loading is low, the ions occupy the β cationic sites, which are located in the twisted eight-membered rings of the mordenite cavity. By increasing the Co/Al ratio, the ions occupy the α-type sites, which are located in the main channel, coordinated with framework oxygens of the six-membered rings. Finally, at high cobalt loadings, the ions occupy the γ-sites, which are located in the "boat-shaped" site of mordenite. Divalent metal ions in these sites are coordinated to six framework oxygens at approximately octahedral coordination. This represents the most highly coordinated site.

In this work, all Ag(*x*)M samples have a reduction peak close to 222 °C with a shoulder at a lower temperature which could correspond to nanoparticles of highly dispersed Ag_2O, in agreement with the Ag_2O/M sample prepared by mechanical mixture (Fig. 1, profile a). Isolated Ag^+ ions sitting in α cationic site could also be reduced in this region, while the reduction at temperatures between 300 °C and 600 °C would correspond to Ag^+ ions exchanged at more stable β cationic sites. In addition, the small reduction peak above

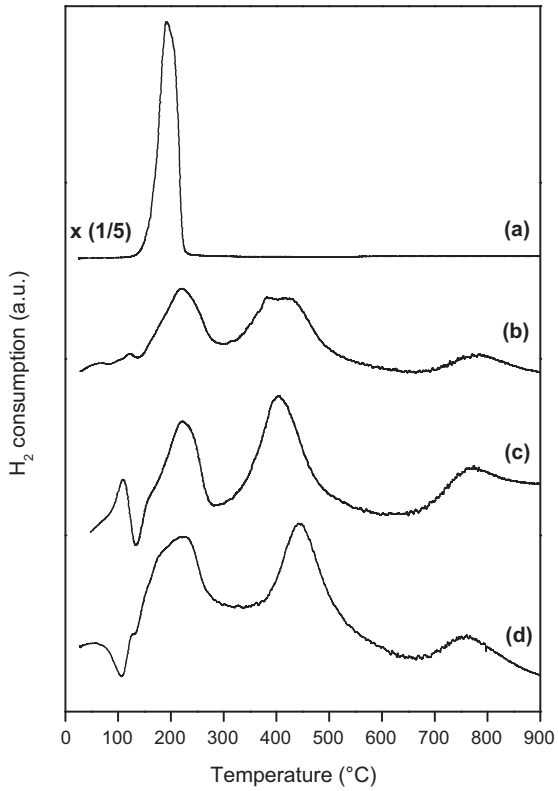

Fig. 1. TPR profiles for (a) Ag_2O/M and calcined (b) Ag(5)M, (c) Ag(10)M and (d) Ag(15)M catalysts.

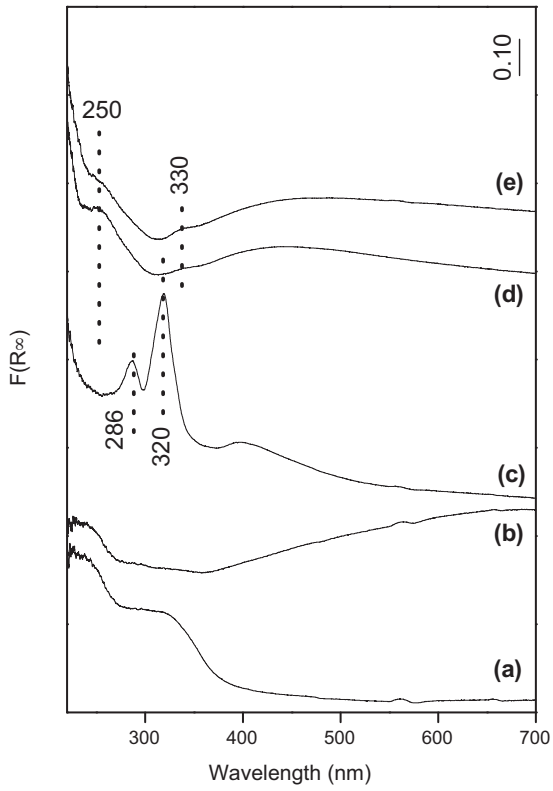

Fig. 2. UV–vis DRS spectra of (a) NaMOR, (b) Ag_2O/M, (c) Ag(5)M, (d) Ag(10)M and (e) Ag(15)M samples.

600 °C could be assigned to Ag^+ ions located at very stable sites with high coordination, like γ-sites, in which the cation strongly interacts with the zeolitic structure. Another hypothesis is to consider that Ag cations (belonging to silver oxides or to isolated exchanged ions) would be readily reduced to Ag cationic clusters (Ag_n^{m+}) at the first peak, and that cationic clusters would further reduce to metal particles at the second and third peaks, as suggested by Shibata et al. [32] who studied the Ag cluster formed in H zeolites during H_2 reduction.

In addition, the population of α-sites increases with the Ag/Al ratio, while it is maximum in Ag(10)M for β cationic sites. For the Ag(5)M and Ag(10)M catalysts, the total H_2/Ag ratio is slightly less than 0.50, probably because when the concentration of silver is low, a fraction of Ag^+ ions occupy the γ cationic sites which are more difficult to reduce. Nevertheless, the complete reduction of all the silver ions at lower temperatures was observed for the sample with 15 wt% Ag. This is probably due to the fact that a higher concentration of metallic silver in this sample can be reduced at temperatures lower that 600 °C during TPR experiment, which would effectively catalyze the H_2 dissociation, thus favoring the reduction of the silver ions located at γ sites.

3.1.3. UV–vis DRS

The electronic spectra of silver in solutions, inert gas, solid matrices and zeolites show that Ag^+ ions and small Ag clusters exhibit characteristic absorption bands in the UV–vis region.

Fig. 2 shows the UV–vis spectra in 220–700 nm region for the Ag(*x*)M catalysts (spectra (c)–(e)), Ag_2O/M prepared by mechanical mixture (spectrum (b)), and NaMOR (spectrum (a)). The Ag(*x*)M samples exhibit an intense UV absorption band at around 220 nm (the peak position of the band may exist in the wavelength region shorter than 200 nm) which is attributed to the [Kr] $4d^{10}$–[Kr] $4d^9 5s^1$ electronic transition on the isolated Ag^+ ions exchanged into NaMOR. Shi et al. [16] reported that three overlapped bands below 230 nm (196, 212 and 224 nm) correspond to the absorption of isolated silver ions exchanged into H-ZSM-5. Also, Shibata et al. [33] reported bands at 210 and 235 nm assignable to Ag^+ ions in Ag-MFI pretreated in a flow of 10% O_2 at 500 °C.

The assignment of individual absorption bands to different silver species in zeolites have been widely discussed in the literature [16,33–35]. The existence of cationic clusters (Ag_n^{m+}), metallic clusters (Ag_n^0) with $n \leq 8$ and isolated Ag^+ ions was proposed, which can absorb energy in the UV–vis region.

In this work, bands at 286, 320 and 400 nm are observed for the Ag(5)M sample. The bands at 286 and 320 nm correspond to small silver cationic clusters ($Ag_n^{\delta+}$, $2 \leq n \leq 4$) [33,36].

The weak band around 370–480 nm could be due to Ag_2O nanoparticles, which display capability of light absorption in both UV and visible range of 200–650 nm [37]. A similar band was observed in the UV–vis spectra of Ag-H-ZSM-5 after pretreatment in O_2/He gas stream [16].

Samples with 10 and 15 wt% Ag exchanged in mordenite, spectra (d) and (e), respectively, have a broad signal at 250 nm and a weak one around 330 nm corresponding to $Ag_n^{\delta+}$ clusters. The absorption signal of silver oxides can also be observed. In (d) and (e) spectra, it is possible that the presence of a greater amount of water molecules coordinated with Ag^+ ions decreases the intensity of the spectra [38].

3.1.4. XPS surface characterization

In order to investigate the chemical state of Ag^+ exchanged species and supported nanoparticles (Ag° and Ag_2O), the Ag 3d photoelectron spectra of Ag(*x*)M as well as those of the Ag_2O/M samples were obtained (Fig. 3A). The Ag 3d spectra of silver exchanged in mordenite show peaks around 368.3 eV and 374.3 eV (FWHM ~ 2.1), which are readily assigned to core-level Ag $3d_{5/2}$ and Ag $3d_{3/2}$ photoemissions, respectively. Besides, the binding energy values shift to 367.8 eV and 373.8 eV for the Ag_2O/M

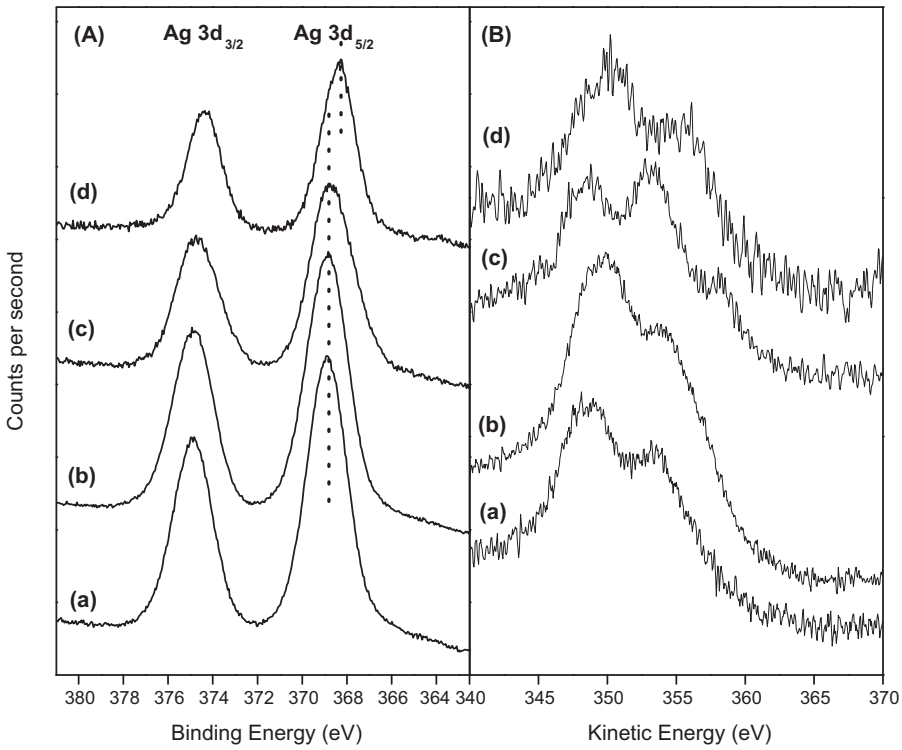

Fig. 3. XPS spectra obtained for calcined (a) Ag(5)M, (b) Ag(10)M (c) Ag(15)M and (d) Ag_2O/M; (A) Ag 3d and (B) Ag M_4VV Auger region.

sample. Taking into account the XPS results of the standard samples previously reported [39], it is highly difficult to discriminate the peak position of Ag $3d_{5/2}$ for Ag_2O (368.4 eV), AgO (368.0 eV) and metallic Ag (368.2 eV); thus, it is uncertain to identify the chemical state of silver sitting in the mordenite structure only from the analysis of Ag 3d electronic level. An additional measure was performed on the Ag M_4VV Auger transition region (Fig. 3B) and the modified Auger parameter (α') was calculated (Table 2). The Auger transition spectra of Ag(x)M samples have a peak with kinetic energy of 354.0–354.5 eV, while for Ag_2O/M it is 357.7 eV; therefore the Auger parameter (α') value results around 722.3 eV for silver-exchanged in mordenite and 724.6 eV for Ag_2O supported, in agreement with Bera et al. [40] who reported values of 726.3 eV and 724.5 eV for Ag° and Ag_2O, respectively. The lower α' values observed for Ag(x)M samples suggest that the silver species are mostly Ag^+ ions at exchange positions. The FWHM values of silver $3d_{5/2}$ peaks for Ag(x)M samples are slightly broader than Ag_2O/M, which indicates the presence of small particles of Ag_2O dispersed in the mordenite structure according to the TPR results. In addition, the BE measured to Al 2p and O 1s core-level were ca. 74.0 eV and 531.7 ± 0.1 eV, respectively for Ag(x)M samples.

Table 2
XPS analysis and modified Auger parameters.

Catalyst	BE	KE	α'[c]	Atomic ratio[d]		
	Ag $3d_{5/2}$[a]	Ag M_4VV[b]		$Si/Al)_S$	$Ag/Al)_S$	$Ag/Al)_B$
Ag(5)M	368.4	354.0	722.3	6.1	0.67	0.18
Ag(10)M	368.3	354.5	722.8	6.1	0.95	0.36
Ag(15)M	368.2	354.0	722.2	6.2	0.91	0.53
Ag_2O/M	367.8	357.1	724.9	6.0	0.30	–

[a] Binding energy (eV).
[b] Kinetic energy (eV).
[c] Modified Auger parameter: α' (eV) = KE (AgM_4VV) − KE ($Ag3d_{5/2}$) + 1253.6 eV.
[d] 'S' represents the atomic surface ratio and 'B' indicates the atomic ratio in the bulk.

The atomic surface ratios $Ag/Al)_S$ and $Si/Al)_S$ calculated from XPS data are presented in Table 2. The high values $Ag/Al)_S$ suggest a surface enrichment with silver in Ag-exchanged mordenite. The Si/Al ratio remains constant around 6.2 close to the bulk value (Si/Al = 6.5).

3.2. Hydrocarbon adsorption and retention capacity

3.2.1. Breakthrough curves

The measure of the breakthrough curves is a direct method to determine the HC adsorption capacity from an adsorbent material. Fig. 4 compares the breakthrough curves for toluene and butane adsorption at 100 °C on NaMOR and samples exchanged with 5, 10 and 15 wt% Ag. When toluene was adsorbed (Fig. 4A), the NaMOR sample showed the greatest adsorption capacity, since the time required to reach saturation was the highest. The incorporation of 5 wt% Ag, results in a notable decrease in the amount of toluene adsorbed, probably due to the decrease in pore volume (see Table 1). Another reason for this decrease could be the exchange of protons during the ionic exchange with silver nitrate solution (pH 5) because it has been reported that Na-mordenite adsorbs more toluene than H-Mordenite [41]. The increase in Ag loading (samples with 10 and 15 wt%) results in an increase in the adsorption capacity, because the Ag interaction with toluene is stronger than with H sites. As a matter of fact, for the Ag(15)M sample the amount of toluene adsorbed is only slightly lower than that for NaMOR.

However, when butane was adsorbed at 100 °C (Fig. 4B), the adsorbed amount decreased for Ag(x)M catalysts compared to the NaMOR support but the breakthrough curves were similar for the exchanged catalysts with different Ag loading. Hence, Table 3 presents the results obtained from the studies of toluene or butane adsorption and desorption in Ag-mordenite catalysts. It presents the micromoles of toluene and butane adsorbed at 100 °C (Q_{ADS}), calculated from breakthrough curves. It can be observed that the NaMOR support and the Ag(x)M samples adsorbed more toluene

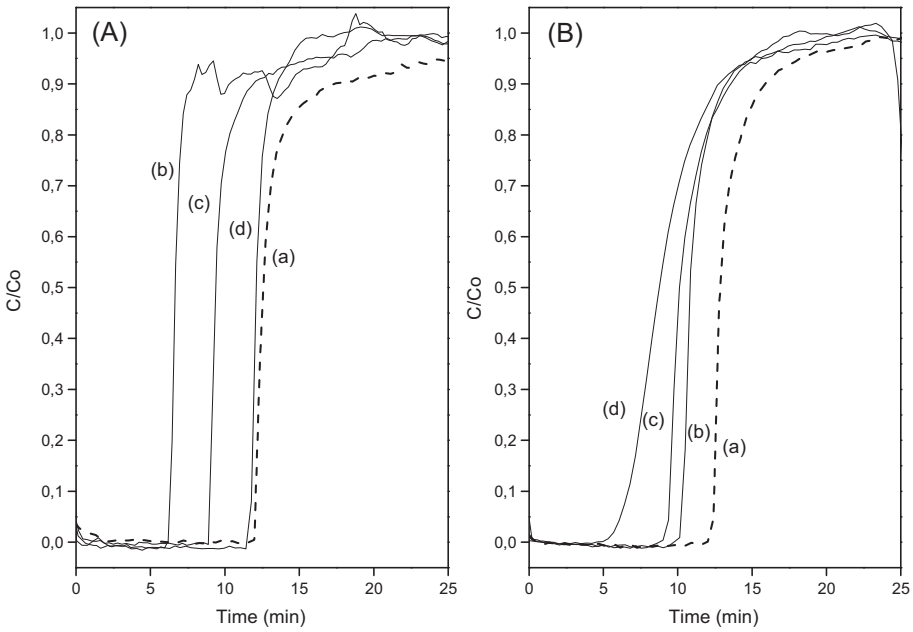

Fig. 4. Breakthrough curves of (A) toluene or (B) butane adsorption at 100 °C on (a) NaMOR, (b) Ag(5)M, (c) Ag(10)M and (d) Ag(15)M catalysts. Conditions: 0.10 g of sample, 20 cm^3 min^{-1} of toluene (8000 ppm) or butane (10,000 ppm) in He.

than butane. The amount of butane was almost similar for the different silver loaded mordenites.

In order to understand these results, it should be taken into account that the substitution of a Si^{4+} ion by an Al^{3+} ion with a lower valence into the Na-mordenite zeolites, produces a negative charge on the structure that is neutralized by the Na^+ cation forming a conjugate acid–base pair. The Na^+ cation acts as a Lewis acid site, while the oxygen of the zeolite structure with partial negative charge acts as a Lewis base [42,43].

The Ag^+ ions present in the prepared samples represent active sites for the adsorption of toluene and butane. However, the presence of different concentrations of silver and the adsorption capacity observed reveals two opposite effects of silver. On the one hand, silver species produce the blocking of the NaMOR channels due to the incorporation of a compensation cation with greater ionic radius; 0.95 Å for Na^+ and 1.26 Å for Ag^+. This effect is directly linked to the loss of crystallinity and textural properties of the supported zeolite (Table 1). On the other hand, a second effect is the strong interaction between silver and the adsorbed hydrocarbon; as a matter of fact, the strength of the interaction strongly depends on the hydrocarbon nature.

In the case of toluene, the experimental results show two situations. First, the adsorption capacity decreases significantly with the addition of 5 wt% Ag compared to that of the NaMOR support. In the latter case, the obstruction effect of silver prevails. However, when adding higher metal content, the adsorption capacity increases due to the prevailing effect of the interaction between Ag^+ ions and toluene compared to the obstruction effect.

In the case of butane, it can be noticed that the addition of 5 wt% Ag produces a decrease in the amount of butane adsorbed compared with that of the NaMOR support. In this latter case, the effect of obstruction is predominant, as observed with toluene. However, when adding higher contents of silver, the amount of butane decreases slightly, indicating that there is no strong interaction between the linear hydrocarbon and Ag^+ ions.

In this sense, it appears that the adsorption capacity is strongly influenced by the interaction between the Ag^+ cation with the π electron cloud of the aromatic ring of toluene. Therefore, the interaction of the CH groups with the linear chain of butane or of the toluene methyl group is weak.

The morphology of the mordenite channels should also influence the adsorption properties of the samples. The structure has 12-membered ring main channels of 6.7 Å × 7 Å, secondary channels with 8 members of 2.9 Å × 5.7 Å and side pockets of 3.4 Å × 4.8 Å. Thus, considering that the kinetic diameter of the toluene molecule is 5.8 Å, the Ag^+ ions located in the main channels (alpha sites) would be the most accessible ones to the adsorption of toluene, while those located in the secondary channel (beta sites) would show steric hindrance. Ions located in the side-pockets (gamma sites) would not be accessible to the molecule of toluene. The quantitative analysis of TPR results can help to gain insight about this effect. It can be observed that beta sites (reduction peak

Table 3
Adsorption, desorption and retention capacity of toluene or butane.

Sample	%Ag	Toluene			Butane		
		Q_{ADS}[a]	Q_{DES}[b]	Φ[c]	Q_{ADS}[a]	Q_{DES}[b]	Φ[c]
NaMOR	0	0.93	0.38	40.9	0.534	0.113	21.2
Ag(5)M	5	0.61	0.17	27.9	0.279	0.066	23.7
Ag(10)M	10	0.73	0.35	47.9	0.276	0.130	47.1
Ag(15)M	15	0.86	0.21	24.4	0.235	0.070	29.8
Ag(15)M red. 300 °C	15	0.84	0.16	19.1	ND	ND	ND

[a] Toluene or butane amount adsorbed at 100 °C (μmol mg^{-1}).
[b] Toluene or butane amount desorbed above 100 °C (μmol mg^{-1}).
[c] Toluene or butane retention capacity above 100 °C; $\Phi = (Q_{DES}/Q_{ADS}) \times 100\%$.

between 300 and 600 °C) represent 30–40% of Ag^+ ions present in the samples. On the other hand, the reduction of Ag^+ ions located in alpha sites ($T < 300$ °C) is overlapped with the reduction of Ag_2O particles, so it is difficult to quantify the amount of exchanged Ag^+ cations located on this site. Nevertheless, it can be observed that the peak reduction occurring at less than 300 °C has a shoulder between 180 and 190 °C that can be assigned to silver oxide species. This shoulder increases with the increasing Ag^+ concentration, indicating that the Ag_2O amount increases with increasing Ag content.

3.2.2. Temperature-programmed desorption of C_7H_8 or C_4H_{10}

Fig. 5 shows the desorption profiles of toluene or butane chemisorbed on NaMOR and samples exchanged with 5, 10 and 15 wt% of silver. When toluene was adsorbed at 100 °C, the NaMOR support (profile a) presented two characteristic zones, one at low temperature, between 170 and 300 °C, and another one between 300 and 500 °C. The region at lower temperature could be associated with weakly adsorbed toluene. In contrast, the HC released at high temperatures could be linked with toluene that interacts more strongly with Na^+ sites. In contrast, when butane was adsorbed on NaMOR, the profile had only one peak at temperatures below 200 °C.

In silver-containing samples, the toluene adsorbed at 100 °C was retained up to temperatures close to 300 °C, while the maximum temperature of butane desorption was always below 200 °C. This could be due to the fact that Ag^+ ions ($[Kr]\ 4d^{10}5\,s^0$) are able to activate the adsorbed toluene containing π electrons through the donation of d electrons to π* antibonding orbitals of toluene molecule [29]. Therefore, the interaction between Ag^+ ions is stronger with the π-electrons of the aromatic ring of the toluene molecule than the σ-electrons of the linear chain of butane.

Comparing the amount of toluene or butane retained in the Ag(*x*)M samples (Fig. 5, Table 3) with the amount retained in the NaMOR support, the addition of silver results in an optimal value of the Φ ratio (Q_{ADS}/Q_{DES}) for the catalyst with 10 wt% Ag. As a matter of fact, it can be seen that the sample with 15 wt% of Ag desorbs a lower amount of toluene than that with 10 wt%. The former sample has a higher content of Ag_2O, which could explain this behavior. Silver oxide does not adsorb toluene, and it could partially block alpha sites located in the main channels, thus decreasing the strength of the interactions with toluene.

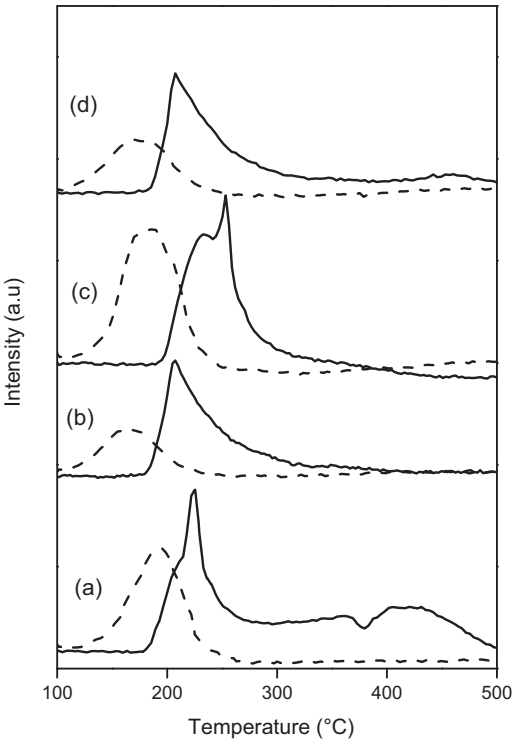

Fig. 5. Profiles of temperature-programmed desorption (TPD) of adsorbed toluene (—) or butane (- - -) on (a) NaMOR, (b) Ag(5)M, (c) Ag(10)M and Ag(15)M catalysts after adsorption at 100 °C with 8000 ppm of C_7H_8/He or 10,000 ppm of C_4H_{10}/He and desorption in He flow with a heating rate 10 °C min^{-1}.

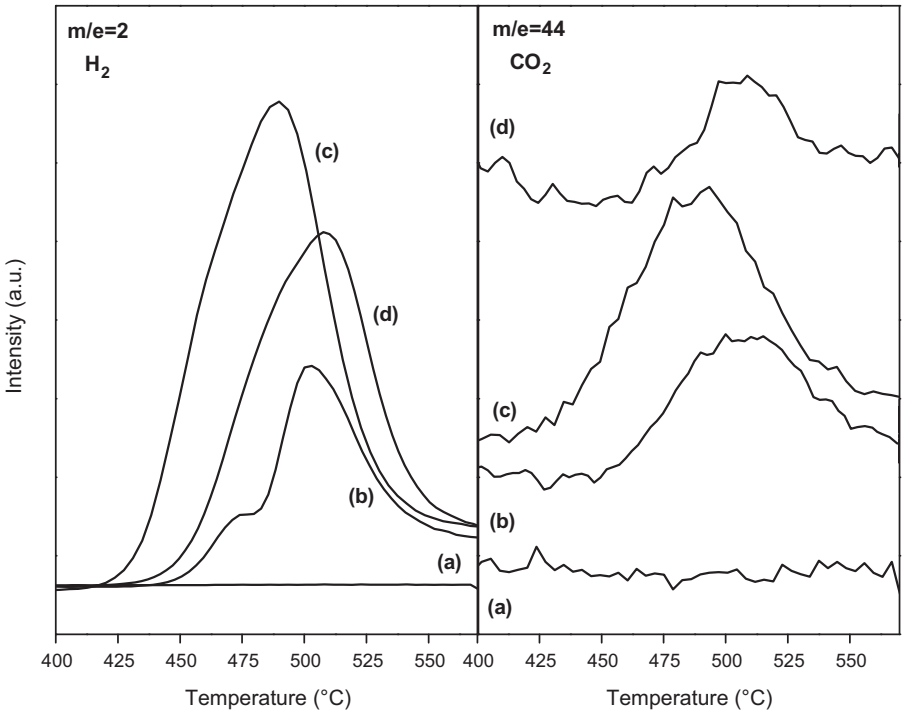

Fig. 6. H_2 and CO_2 profiles obtained during the toluene desorption temperature programmed to (a) NaMOR, (b) Ag(5)M, (c) Ag(10)M and (d) Ag(15)M samples.

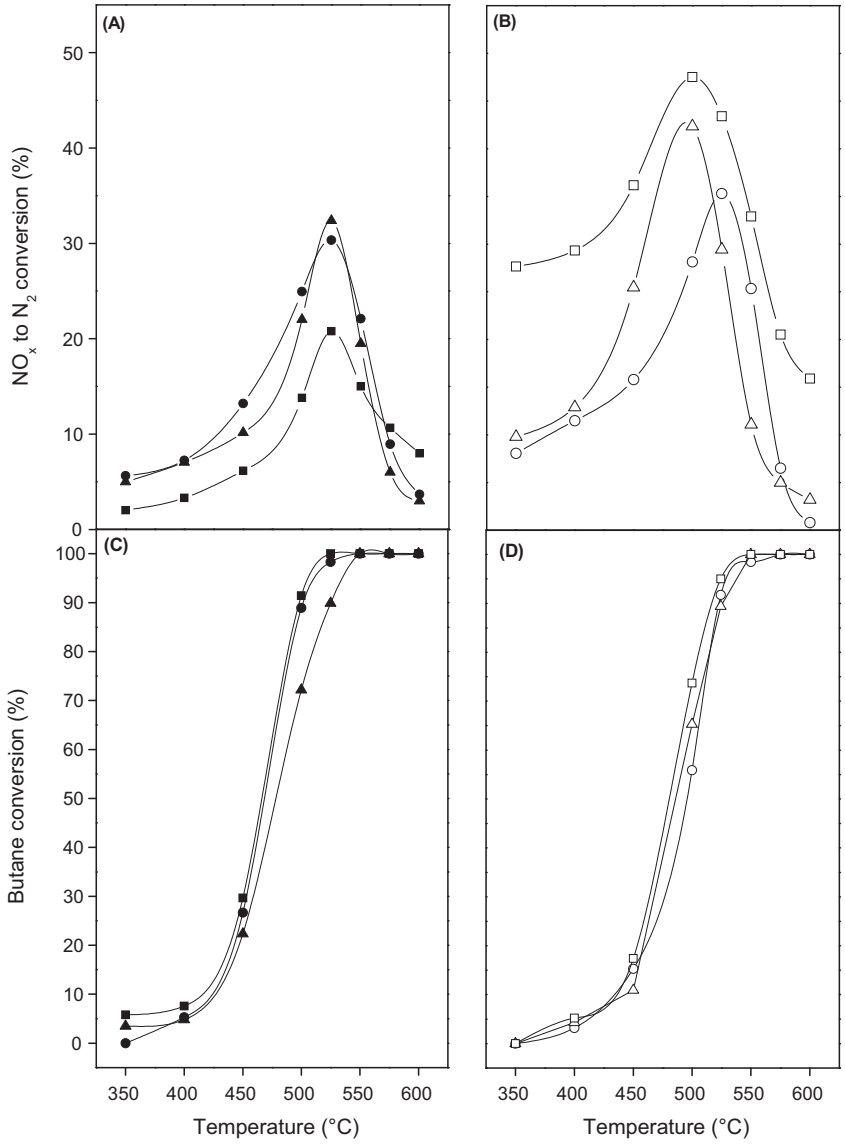

Fig. 7. The SCR of NO_x using Ag(x)M samples: (●, ○) 5 wt% Ag; (▲, Δ) 10 wt% Ag and (■, □) 15 wt% Ag. Reaction conditions: GHSV = 20,000 h^{-1}, 1000 ppm NO, 2% O_2, 500 ppm C_4H_{10}. Filled symbols: 0% H_2O, Empty symbols: 2% H_2O. (A and B) NO_x to N_2 conversion; (C and D) C_4H_{10} conversion as a function of temperature.

It was also noticed that the Ag(x)M samples did not exhibit the second peak of toluene desorption between 300 and 500 °C. In this region, the appearance of signals corresponding to H_2, CO_2 and H_2O was observed during the temperature-programmed desorption of toluene but were not detected with butane. Fig. 6 shows the desorption profiles of hydrogen and CO_2 obtained for the NaMOR support (profile a) and exchanged samples with 5, 10 and 15 wt% Ag (profiles b–d).

When the temperature was 500 °C, the highest of the peaks corresponding to hydrogen and water could be observed. These compounds are observed only in the samples exchanged with silver and there are no other decomposition products. In this vein, Rönkkönen et al. [44] reported the aromatic hydrocarbon decomposition reactions on Rh, Ni, Pt or Pd supported on ZrO_2. In addition, Ding et al. [45] studied the methane activation over Ag-exchanged ZSM5 zeolites for H_2 formation.

Therefore, toluene probably interacts strongly with Ag^+ ions and is retained by them up to 350 °C and a higher temperature, the toluene decomposition mainly occurs producing coke and hydrogen, by means of the following reaction [46]:

$$C_7H_8 \rightarrow 7C(s) + 4H_2(g) \quad (I)$$

The generation of carbon dioxide is linked to the oxidation reaction of toluene. Table 3 also shows the toluene adsorption and desorption values obtained on Ag(15)M reduced in H_2 flow at heating rate of 5 °C min^{-1} from room temperature to 300 °C and then, swept with an inert flow to the adsorption temperature. The amount of hydrocarbon adsorbed before and after reducing the Ag_2O species is the same. However, the amount of toluene retained is minor in comparison to the calcined Ag(15)M. The retention capacity decreased about 22% for the reduced sample. Therefore, it follows that Ag_2O species are probably not specifically involved in the process of toluene adsorption but are important to improve the retention ability. The strong interaction between toluene and the Ag_2O sites very likely promotes the partial oxidation of toluene at high temperatures (≈500 °C), by means of the following reaction:

$$C_7H_8 + 18Ag_2O \rightarrow 7CO_2 + 4H_2O + 36Ag^\circ \quad (II)$$

3.3. Catalytic tests

Figs. 7 and 8 show the conversion of NO_x to N_2 and the hydrocarbon conversions for the SCR in the presence of oxygen excess. The catalytic performance was analyzed in the absence and

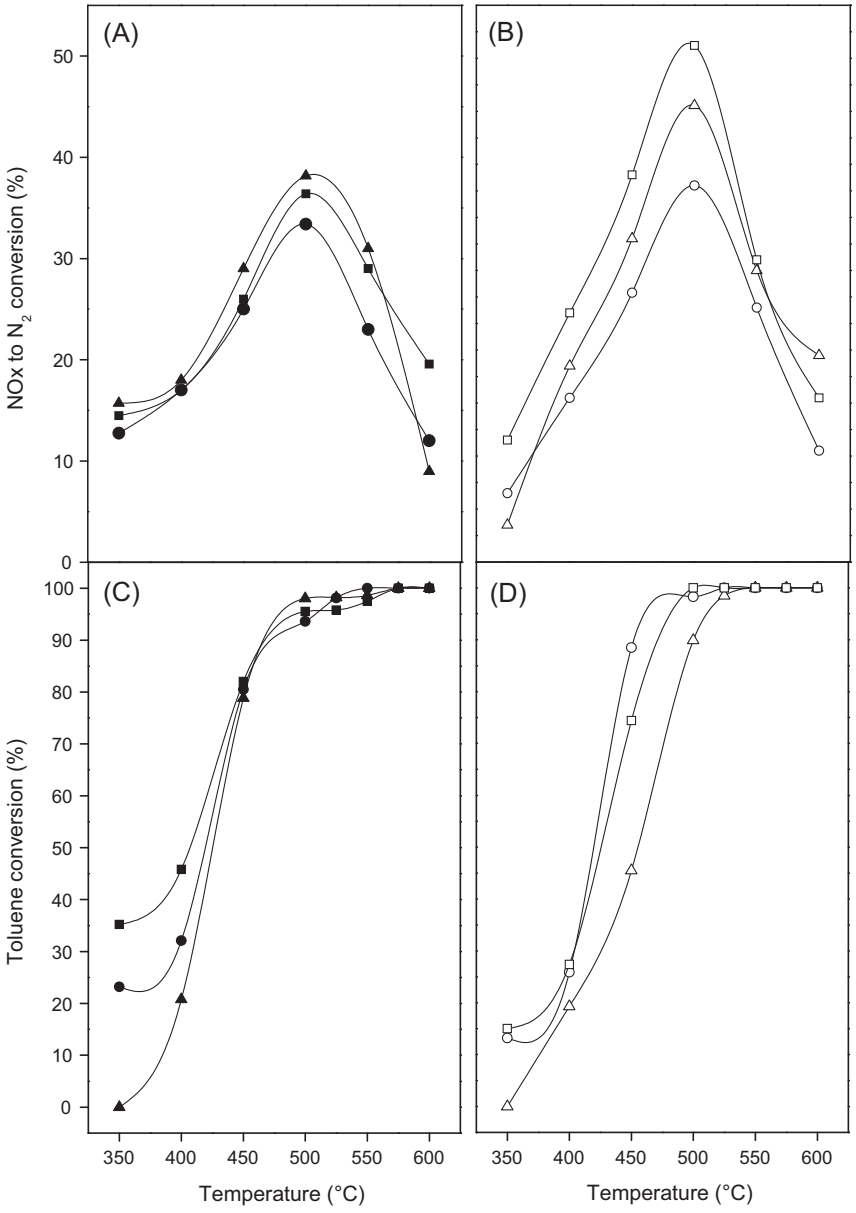

Fig. 8. The SCR of NO_x using Ag(x)M samples: (●, ○) 5 wt% Ag; (▲, Δ) 10 wt% Ag and (■, □) 15 wt% Ag. Reaction conditions: GHSV = 20,000 h^{-1}, 1000 ppm NO, 2% O_2, 500 ppm C_7H_8. Filled symbols: 0% H_2O, Empty symbols: 2% H_2O. (A and B) NO_x to N_2 conversion; (C and D) C_4H_{10} conversion as a function of temperature.

presence of 2% H_2O. All the catalysts gave volcano-type curves for NO conversion, the peak temperature varying between 500 and 525 °C according to the catalysts and hydrocarbons used.

Under dry reaction conditions with butane (Fig. 7A), the catalysts with 5 and 10 wt% of Ag showed similar activity, the maximum conversion being at 525 °C are 30.3 and 32.4%, respectively. However, in Ag(15)M the NO reduction activity was lower. When the hydrocarbon used was toluene (Fig. 8A), Ag(10)M was also the best catalyst, reaching 38.2% at 500 °C. The activity enhancement displayed using toluene could be due to the higher C/N ratio, i.e. C/N = 3.5 versus C/N = 2 (butane). It is also possible that the toluene aromatic ring was more reactive than the aliphatic chain of butane.

Therefore, in agreement with other authors [47], the maximum conversion to N_2 shows that there is an optimal value between 5 and 10 wt% of Ag under dry conditions.

On the other hand, the effect on the NO reduction activity of adding 2% H_2O was positive. The maximum conversion of NO_x increased from 20% (in dry condition) to 47.5% at 500 °C using butane on Ag(15)M (Fig. 7B). Also, with toluene the NO conversions were greater than those under dry conditions. The highest NO conversion was 51.2% and it was observed at 500 °C over the Ag(15)M catalysts (Fig. 8B). The butane conversions (presented in Fig. 7C and D) were similar for all catalysts and the hydrocarbon total conversion was raised close to 525 °C when the nitrogen conversion was maximum. In the case where toluene was used, the Ag(10)M catalyst showed a toluene conversion lower than the other catalysts at temperatures <450 °C in dry conditions. However in the presence of water, the toluene conversion was the lowest in the whole temperature range (Fig. 8C and D).

In a previous work [48], we studied the effect of water on the NO_x SCR reaction. In agreement with other authors, we concluded that water can participate in different ways: (i) reversibly inhibiting the catalytic reaction, because it adsorbs at the active sites preventing the NO_x adsorption, (ii) water promotes the steam reforming of hydrocarbons and/or (iii) it helps to maintain the surface clean from

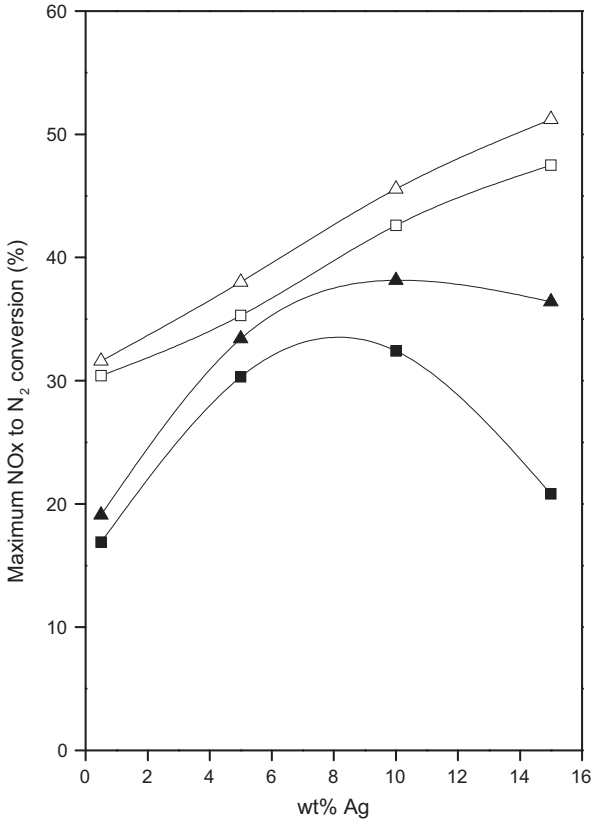

Fig. 9. Influence of Ag loading in the maximun NO to N_2 conversion with HCs: (■, □) 500 ppm butane; (▲, Δ) 500 ppm toluene. Reaction conditions: GHSV = 20,000 h^{-1}, 1000 ppm NO, 2% O_2. Filled symbols: 0% H_2O; empty symbols: 2% H_2O.

carbon deposits. In that work, we demonstrated that in the case of Co exchanged catalysts the latter option is the most important one.

Fig. 9 shows the influence of metal loading on the conversion to N_2 with butane or toluene in the presence or absence of 2% H_2O. Under dry conditions, the conversion of NO to N_2 has an optimum value between 5 and 10 wt% Ag for both hydrocarbons. However, a different behavior was observed with 2% H_2O. Possibly, the steam reforming of hydrocarbon could occur, because it became thermodynamically favorable at temperatures higher than 400 °C. The carbon deposition could take place simultaneously due to decomposition of hydrocarbon and/or by CO disproportionation [49].

Our SCR results on Ag exchanged samples showed that the activity was higher in the presence of water, and we can conclude that the beneficial effect of water is probably due to the production of H_2 from steam reforming, which in turn could improve NO_x reduction, and because water contributes to maintain the surface clean from carbon deposits.

However, due to the complexity of the reaction system, a high number of parallel and consecutive reactions can take place under reaction conditions, which prevents the steam reforming of hydrocarbon from being independently measured.

4. Conclusions

Catalysts based on Ag-Mordenite are able to adsorb toluene or butane at low temperature and to retain them up to temperatures of 250 and 180 °C, respectively. During the TPD experiments, besides hydrocarbon desorption, other interesting features are observed for toluene that are not seen in the case of butane. Since toluene molecules are retained at higher temperature, a fraction of them are decomposed to give hydrogen, carbon, carbon dioxide and water, through complex reactions that probably involve the hydrocarbon decomposition and Ag^+ reduction with toluene and/or hydrogen molecules.

Even though at high temperatures, the studied catalysts have a good NO_x reduction activity with toluene and butane in the presence of water, with a maximum conversion to N_2 of 51.2 and 47.5%, respectively, at 525 °C in both cases.

In the active catalysts, small highly dispersed Ag_2O particles are present in coexistence with isolated Ag^+ ions and/or small clusters of Ag^+ cations located at the mordenite exchange sites.

Regarding toluene adsorption, the presence of silver has two opposite effects: the chemical interaction with the hydrocarbon molecules and a partial obstruction of the mordenite channels. The interaction between Ag^+ at exchange positions with toluene is stronger than with butane due to the presence of π electrons in the aromatic ring. As a result of this strong interaction, toluene is retained at high temperatures and decomposes generating products such as coke and hydrogen. Besides, part of the retained toluene reacts with silver oxide species to produce water and CO_2.

Acknowledgements

The authors acknowledge the financial support received from UNL and CONICET. They are also grateful to ANPCyT for the purchase of the SPECS multitechnique analysis instrument (PME8-2003), the Laser Raman Spectrometer (PME Grant 36 985 87-PAE), and the UV–vis spectrometer (PME 311). Thanks are given to Prof. Elsa Grimaldi for the English language editing.

Appendix A. Supplementary data

Supplementary data associated with this article can be found, in the online version, at doi:10.1016/j.apcata.2011.08.033.

References

[1] P. Bazin, O. Marie, M. Daturi, Stud. Surf. Sci. Catal. 171 (2007) 97–143.
[2] Y. Li, J.N. Armor, Appl. Catal. B: Environ. 1 (1992) 221–256.
[3] V.I. Parvulescu, P. Grange, B. Delmon, Catal. Today 46 (1998) 223–231.
[4] R.M. Heck, R.J. Farrauto, Catalytic Air Pollution Control: Commercial Technology, Van Nostrand Reinhold, New York, 1995.
[5] P.J. Wesson, R.Q. Snurr, Microp. Mesop. Mater. 125 (2009) 35–38.
[6] K.F. Czaplewski, T.L. Reitz, Y.J. Kim, R.Q. Snurr, Microp. Mesop. Mater. 56 (2002) 55–64.
[7] H.Y. Chen, X. Wang, W.M.H. Sachtler, Appl. Catal. A: Gen. 194/195 (2000) 159–168.
[8] A. Kubacka, J. Janas, E. Wloch, B. Sulikowski, Catal. Today 101 (2005) 139–145.
[9] R.M. Serra, E.E. Miró, A.V. Boix, Microp. Mesop. Mater. 127 (2010) 182–189.
[10] N.R. Bruke, D.L. Trimm, R.F. Howe, Appl. Catal. B: Environ. 46 (2003) 97–104.
[11] J.H. Park, S.J. Park, I.S. Nam, G.K. Yeo, J.K. Kil, Y.K. Youn, Microp. Mesop. Mater. 101 (2007) 264–270.
[12] H.X. Li, J.M. Donohue, W.E. Chrmier, Y.F. Chu, Stud. Surf. Sci. Catal. 158 (2005) 1375–1382.
[13] D. Barthomeuf, Catal. Rev. 38 (1996) 521–612.
[14] T. Kanasawa, Catal. Today 96 (2004) 171–177.
[15] T.H. Yeon, H.S. Han, E.D. Park, J.E. Yie, Microp. Mesop. Mater. 119 (2009) 349–355.
[16] C. Shi, M. Cheng, Z. Qu, X. Bao, J. Mol. Catal. A: Chem. 235 (2005) 35–43.
[17] T. Furusawa, K. Seshan, J.A. Lercher, L. Lefferts, K. Aika, Appl. Catal. B: Environ. 37 (2002) 205–216.
[18] R. Zhang, S. Kaliaguine, Appl. Catal. B: Environ. 78 (2008) 275–287.
[19] R.M. Heck, R.J. Farrauto, Appl. Catal. A: Gen. 221 (2001) 443–457.
[20] M.L.M. Oliveira, A.A.L. Miranda, C.M.B.M. Barbosa, C.L. Cavalcante Jr., D.C.S. Azevedo, E. Rodriguez-Castellón, Fuel 88 (2009) 1885–1892.
[21] Z. Sarshar, M.H. Zahedi-Niaki, Q. Huang, M. Eic, S. Kaliaguine, Appl. Catal. B: Environ. 89 (2009) 37–45.
[22] S.P. Elangovan, M. Ogura, S. Ernst, M. Hartmann, S. Tontisirin, M.E. Davis, T. Okubo, Microp. Mesop. Mater. 96 (2006) 210–215.
[23] B. Lippens, B. Linsen, J. de Boer, J. Catal. 3 (1964) 32–37.
[24] M.L. Mignoni, D.I. Petkowicz, N.R.C. Fernandez Machado, S.B.C. Pergher, Appl. Clay Sci. 41 (2008) 99–104.
[25] J.T. Wolan, G.B. Hoflund, Appl. Surf. Sci. 125 (1998) 251–258.
[26] Database of Balzers Quadstar 433 V6.0 Software.
[27] Zeolyst International, Available from: http://www.zeolyst.com.

[28] A. Ausavasukhi, S. Suwannaran, J. Limtrakul, T. Sooknoi, Appl. Catal. A: Gen. 345 (2008) 89–96.
[29] E. Kukulska-Zaja, J. Datka, Microp. Mesop. Mater. 109 (2008) 49–57.
[30] L. Capek, J. Dedecek, P. Sazama, B. Wichterlová, J. Catal. 272 (2010) 44–54.
[31] D. Kaucky, A. Vondrová, J. Dedecek, B. Wichterlová, J. Catal. 194 (2000) 318–329.
[32] J. Shibata, Y. Takada, A. Shichi, S. Satokawa, A. Satsuma, T. Hattori, Appl. Catal. B: Environ. 54 (2004) 137–144.
[33] J. Shibata, Y. Takada, A. Shichi, S. Satokawa, A. Satsuma, T. Hattori, J. Catal. 222 (2004) 368–376.
[34] V.S. Gurin, V.P. Petranovskii, M.A. Hernandez, N.E. Bogdanchikova, A.A. Alexeenko, Mater. Sci. Eng. A 391 (2005) 71–76.
[35] R. Bartolomeu, C. Henriques, P. da Costa, F. Ribeiro, Catal. Today (2011), doi:10.1016/j.cattod.2011.02.009, in press.
[36] N.E. Bogdanchikova, V.P. Petranovskii, R. Machorro M., Y. Sugi, V.M. Soto G., S. Fuentes M., Appl. Surf. Sci. 150 (1999) 58–64.
[37] W. Zhou, H. Liu, J. Wang, D. Liu, G. Du, J. Cui, Appl. Mater. Interf. 2 (2010) 2385–2392.
[38] R. Seifert, R. Rytz, G. Calzaferri, J. Phys. Chem. A 104 (2000) 7473–7483.
[39] A. Naydenov, P. Konova, Pen. Nikolov, F. Klingstedt, N. Kumar, D. Kovacheva, P. Stefanov, R. Stoyanova, D. Mehandjiev, Catal. Today 137 (2008) 471–474.
[40] S. Bera, P. Gangopadhyay, K.G.M. Nair, B.K. Panigrahi, S.V. Narasimhan, J. Elec. Spectr. Rel. Phen. 152 (2006) 91–95.
[41] R.M. Serra, E.E. Miró, P. Bolcatto, A.V. Boix, Microp. Mesop. Mater. (2011), doi:10.1016/j.micromeso.2011.05.016.
[42] Y. Yu, G. Xiong, C. Li, F. Xiao, Microp. Mesop. Mater. 46 (2001) 23–34.
[43] Y. Oumi, T. Kanai, B. Lu, T. Sano, Microp. Mesop. Mater. 101 (2007) 127–133.
[44] H. Rönkkönen, P. Simell, M. Reinikainen, O. Krause, M. Niemelä, Fuel 89 (2010) 3272–3277.
[45] B. Ding, S. Huang, W. Wang, Appl. Surf. Sci. 254 (2008) 4944–4948.
[46] E. Kantaris, P. Donaj, W. Yang, A. Zabaniotou, J. Hazard. Mater. 167 (2009) 675–684.
[47] K. Shimizu, J. Shibata, H. Yoshida, A. Satsuma, T. Hattori, Appl. Catal. B: Environ. 30 (2001) 151–162.
[48] A.V. Boix, S.G. Aspromonte, E.E. Miró, Appl. Catal. A: Gen. 341 (2008) 26–34.
[49] D. Swierczynski, C. Courson, A. Kiennemann, Chem. Eng. Processing: Proc. Int. 47 (2008) 508–513.